ESKİŞEHİR TEKNİK ÜNİVERSİTESİ BİLİM VE TEKNOLOJİ DERGİSİ B- TEORİK BİLİMLER

Eskişehir Technical University Journal of Science and Technology B- Theoretical Sciences

2023, 11(1), pp. 13-28, DOI: 10.20290/estubtdb.1080946

RESEARCH ARTICLE

OPTICAL CHARACTERIZATION of STEARIC ACID POWDER and ITS USE for THE SYNTHESIS of NANOPARTICLES

Çağdaş ALLAHVERDİ [1,*]

[1] Department of Software Engineering, Faculty of Engineering, Toros University, Mersin, Turkey

ABSTRACT

Fatty acids are found in the structure of triglycerides and phospholipids which have vital importance for the life. Stearic acid is an important member of the fatty acids. It is used in the manufacturing of various products such as soaps, detergents, and rubbers. It is valuable to provide a thermal and optical characterization database of stearic acid. In this study, a comprehensive database has been prepared by studying thermogravimetric analysis, X-ray powder diffraction, dispersive Raman and Fourier transform infrared spectroscopies of stearic acid. Its thermal decomposition temperature, X-ray diffraction angles and infrared vibrational modes have been determined. Stearic acid has been used at the synthesis of cadmium selenide quantum dots, bismuth nanoparticles and mixed copper/zinc nanocrystals. Hot-injection and one-pot synthesis methods have been utilized to synthesize these nanostructures. Their sizes, distributions, shapes, elemental compositions, and crystalline structures have been investigated by transmission electron microscopy and energy dispersive X-ray analysis. Mixed copper/zinc nanocrystals have also been examined by X-ray diffraction spectroscopy.

Keywords: Stearic acid, Optical characterization, Chemical synthesis, Quantum dots, Nanoparticles

1. INTRODUCTION

Stearic acid is an important long chain fatty acid. It is also called as octadecanoic acid. It is found naturally in various animal and vegetable fats and oils [1]. The structure of a stearic acid molecule is illustrated in Figure 1. As seen from Figure 1, it consists of 18 carbon, 36 hydrogen and 2 oxygen atoms and its molecular formula is $C_{18}H_{36}O_2$. It has no carbon-carbon double bond, and therefore it is a saturated fatty acid. Hydrocarbon part of a stearic acid, that is its tail ($C_{17}H_{35}$), is linear and gives hydrophobic property to this molecule. The remaining COOH is the hydrophilic head. Hence, stearic acid molecules can attach to a variety of surfaces with their heads and imparts hydrophobicity or even superhydrophobicity to these surfaces [2-4].

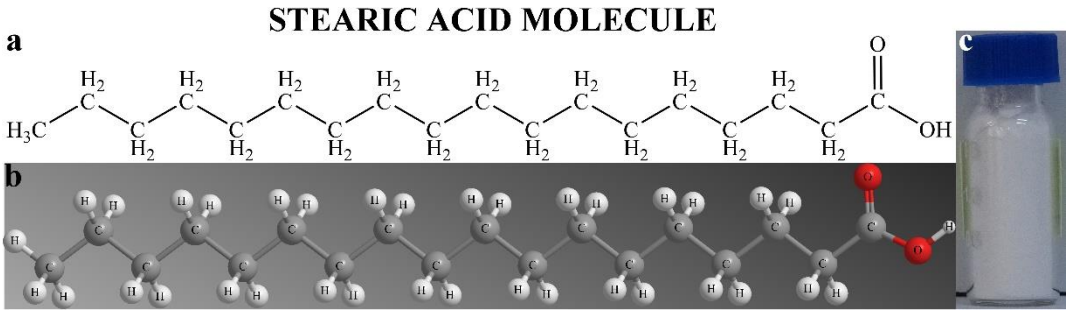

Figure 1. Stearic acid molecule. Structural formula of stearic acid molecule (a), its ball-and-stick model (b) and stearic acid powder in a vial (c).

*Corresponding Author: cagdas.allahverdi@toros.edu.tr
Received: 01.03.2022 Published: 28.02.2023

Self-assembly of these molecules has been studied by some groups [5-7]. Stearic acid is used as dispersant, filler, softener, activator, and lubricant in the industry [8-12]. It is known that stearic acid and zinc oxide cause sulfur vulcanization of rubber [13]. Smooth appearance of pharmaceutical tablets such as paracetamol is obtained by using stearic acid in the formulation [14]. Stearic acid molecules used as ligands of micron sized particles and nanoparticles have attracted attention [15-17]. The attached molecules to the surface of these particles give not only different mechanical properties but also thermal and optical properties to the particles. For example, high quantum efficiencies have been obtained for stearic acid coated semiconductor quantum dots due to its long carbon chain [18]. Better dispersibility has also been obtained when mixing them into some polymers [19]. Some general physical properties of stearic acid are listed at Table 1 [20]. Since stearic acid has a higher melting point and viscosity than many other fatty acids such as oleic, myristic and palmitic acids, the temperature and mixing speed required for nanoparticle synthesis are slightly increased when it is preferred.

Table 1. Physical properties of stearic acid.

Stearic Acid	
Physical Property	**Value**
Appearance	White solid
Molar Mass	284.48 g/mol
Density	0.837 g/cm^3
Viscosity	12 cSt at 70^{o}C
Melting Point	69.6^{o}C
Refractive Index	1.4337

In this study, thermal and optical properties of stearic acid molecules are investigated via their thermogravimetric analysis (TGA), X-ray powder diffraction (XRD), dispersive Raman and Fourier transformed infrared (FTIR) spectroscopies. The usage and role of stearic acid in the chemical synthesis of stearic acid coated nanoparticles are shown and discussed. Cadmium selenide quantum dots, bismuth nanoparticles, mixed copper/zinc nanocrystals are synthesized owing to the fact that cadmium selenide quantum dots, bismuth nanoparticles and copper/zinc nanocrystals have a superior photoluminescence in the visible spectrum range, X-ray and gamma-ray shielding capability, and catalytic properties, respectively [21-23]. Non-aggregated forms of these synthesized nanoparticles are observed in their transmission electron microscopy (TEM) photographs. Thus, stearic acid molecules are used as a successful dispersant agent at the synthesis of these nanoparticles. This finding is valuable because aggregations diminish or extinguish novel properties of nanoparticles as in photoluminescence quantum yield of cadmium selenide quantum dots.

2. EXPERIMENTAL MATERIALS, METHOD and CHARACTERIZATION

2.1. Experimental Materials

Cadmium oxide (≥99.99%), selenium (99.99%), bismuth(III) acetate (≥99.99%), copper(II) acetate monohydrate (99.99%), zinc stearate (10-12% zinc basis), stearic acid (reagent grade, 95%), 1-octadecanol (99%), trioctylphosphine (90%), 1-octadecene (90%), ethyl acetate (99.9%), anhydrous chloroform (≥99%), methanol (≥99.9%) and toluene (≥99.9%) were purchased from Merck (Sigma-Aldrich). The chemicals were used in the experiments without any purification.

2.2. Method

Cadmium selenide (CdSe) quantum dots and bismuth (Bi) nanoparticles were synthesized using hot-injection method [24-26]. Mixed copper/zinc (Cu/Zn) nanocrystals were synthesized using one-pot

method [27]. All chemical reactions were done under a controlled pure argon gas (>99.999%) atmosphere without oxygen.

2.2.1. Preparation of Stearic acid powder

Stearic acid flakes were ground by using porcelain mortar and pestle for further characterizations.

2.2.2. Preparation of CdSe quantum dots

Cadmium oxide was mixed with stearic acid and 1-octadecene in a flask. Mole ratio of stearic acid to cadmium oxide was ~2.98. This mixture was heated to 302ºC under a vigorous stirring. Selenium was mixed and stirred with trioctylphosphine in another flask, heated to 154ºC and then cooled to room temperature. Mole ratio of trioctylphosphine to selenium was ~2.0. Obtained trioctylphosphine-selenium complex was injected rapidly to cadmium oxide-stearic acid-octadecene mixture at 302ºC. Afterwards, the temperature was lowered to 272ºC and CdSe quantum dots were growth at this temperature for a while. CdSe quantum dots were taken from the solution, washed with methanol. CdSe quantum dots were precipitated with centrifugation and then dispersed in toluene for further characterizations.

2.2.3. Preparation of Bi nanoparticles

Bismuth(III) acetate was mixed with stearic acid and 1-octadecene in a flask. Mole ratio of stearic acid to bismuth(III) acetate was ~4.5. This mixture was heated to 151ºC under a vigorous stirring. Selenium was mixed and stirred with trioctylphosphine in another flask, heated to 132ºC and then cooled to 76ºC. Mole ratio of trioctylphosphine to selenium was ~2.0. Obtained trioctylphosphine-selenium complex was injected rapidly to bismuth acetate-stearic acid-octadecene mixture at 151ºC. Afterwards, the temperature was raised to 160ºC and Bi nanoparticles were growth at this temperature for a while. Bi nanoparticles were taken from the solution, washed with methanol and anhydrous chloroform. Bi nanoparticles were precipitated with centrifugation and then dispersed in toluene for further characterizations.

2.2.4. Preparation of mixed Cu/Zn nanocrystals

Copper(II) acetate monohydrate and zinc stearate were mixed with 1-octadecanol and 1-octadecene in a flask. The mole ratio of copper(II) acetate monohydrate to zinc stearate and 1-octadecanol were ~1.00 and ~0.10, respectively. This mixture was stirred and heated up to 308ºC and then cooled to room temperature. Mixed Cu/Zn nanocrystals were precipitated from the solution via centrifugation by using ethyl acetate and methanol and then dispersed in toluene for further characterizations.

2.3. Characterization

TGA was performed with Mettler Toledo TGA/DSC 3+ under nitrogen atmosphere. XRD spectra were recorded using Rigaku SmartLab X-ray diffractometer. X-ray tube voltage and current were set to 40 kV and 30 mA, respectively. Cu K-α radiation (1.541862 Å) was used to scan the samples. FTIR measurement was performed via PerkinElmer Spectrum 400 FT-IR spectrometer with attenuated total reflection (ATR) accessory. Dispersive Raman spectrum was collected with Renishaw inVia Raman microscope at excitation wavelength of 633 nm. TEM photos of nanoparticles were taken with JEOL JEM-2100F at acceleration voltage of 200 kV. JEOL JSM-7600F scanning electron microscope (SEM) with Oxford Inca energy-dispersive X-ray (EDX) system was used for SEM-EDX measurements. Experimental parameters of the measurements are written in the figure captions.

3. RESULTS and DISCUSSION

TGA curve of stearic acid is given at Figure 2. TGA was conducted between 25-650ºC. A slight increase in mass occurs until 199ºC, afterwards mass loss begins and continues up to 585ºC. Here, the onset temperature is found to be 286ºC which shows the initial temperature of thermal decomposition of stearic acid. The highest mass loss rate is observed at ~324ºC which corresponds to the minimum of first derivative of mass loss curve (d(Mass loss)/dT). The offset temperature indicating completion of thermal decomposition is found to be 340ºC. XRD spectrum of stearic acid is shown in Figure 3. This spectrum was measured between 10º-80º. Two strong XRD peaks are determined in this range. These peaks having row numbers 6 and 8 in the spectrum are located at 21.48º and 24.06º, respectively. The local maxima of appearing all XRD peaks are listed at Table 2. Raman spectrum of stearic acid is seen at Figure 4. The wavenumbers of all Raman peaks are determined and listed in Table 2. The highest seven intensities occur at 2881.91 cm^{-1}, 2846.41 cm^{-1}, 2925.31 cm^{-1}, 1296.35 cm^{-1}, 1063.39 cm^{-1}, 1438.61 cm^{-1} and 1130.37 cm^{-1}. These Raman peaks are designated with numbers of 31, 30, 32, 17, 13, 20 and 15 in Figure 4, respectively. According to the literature, these intensive peaks can be ascribed to asymmetric stretching vibration of CH_2 (methylene group), symmetric stretching vibration of CH_2, asymmetric stretching vibration of CH_2, torsional vibration of CH_2, stretching vibration of C-C, bending vibrations of CH_2 and CH_3, and stretching vibration of C-C, respectively [28, 29]. FTIR spectrum of stearic acid is seen at Figure 5. The wavenumbers of observed transmittance valleys are given at Table 2. The seven valleys having lowest transmittance appear at 2915 cm^{-1}, 2848 cm^{-1}, 1699 cm^{-1}, 1298 cm^{-1}, 942 cm^{-1}, 719 cm^{-1} and 729 cm^{-1}. These FTIR bands correspond to the valleys marked with numbers 42, 40, 36, 28, 16, 9 and 10 in Figure 5, respectively. The intensive bands located at 2915 cm^{-1} (42), 2848 cm^{-1} (40) and 1699 cm^{-1} (36) can be referred to asymmetric stretching vibration of CH_2, symmetric stretching vibration of CH_2 and stretching vibration of C=O, respectively [30, 31]. It is evident that symmetric and asymmetric vibrations of methylene group of stearic acid can be observed easily at both spectra, when FTIR and Raman spectra of stearic acid are compared to each other.

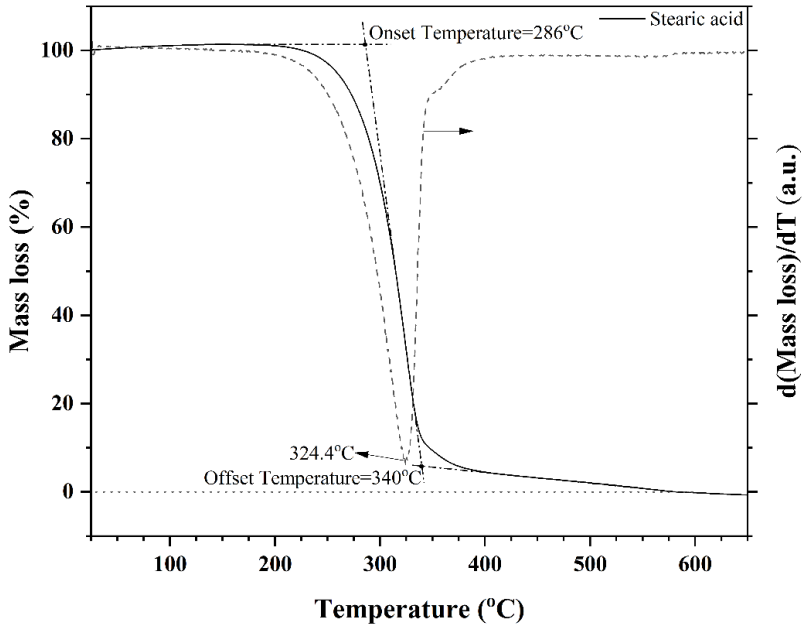

Figure 2. TGA curve of stearic acid. The mass of the sample was 10.5180 mg. The temperature was increased 10ºC per minute from 25ºC to 650ºC. The flow rate of N_2 gas was 40 mL per minute. Solid curve shows mass loss percentage (%) and dashed curve shows first derivative of the mass loss with respect to temperature (d(Mass loss)/dT). Extrapolated lines are indicated with dash-dotted (-·-·) lines to determine onset and offset temperatures.

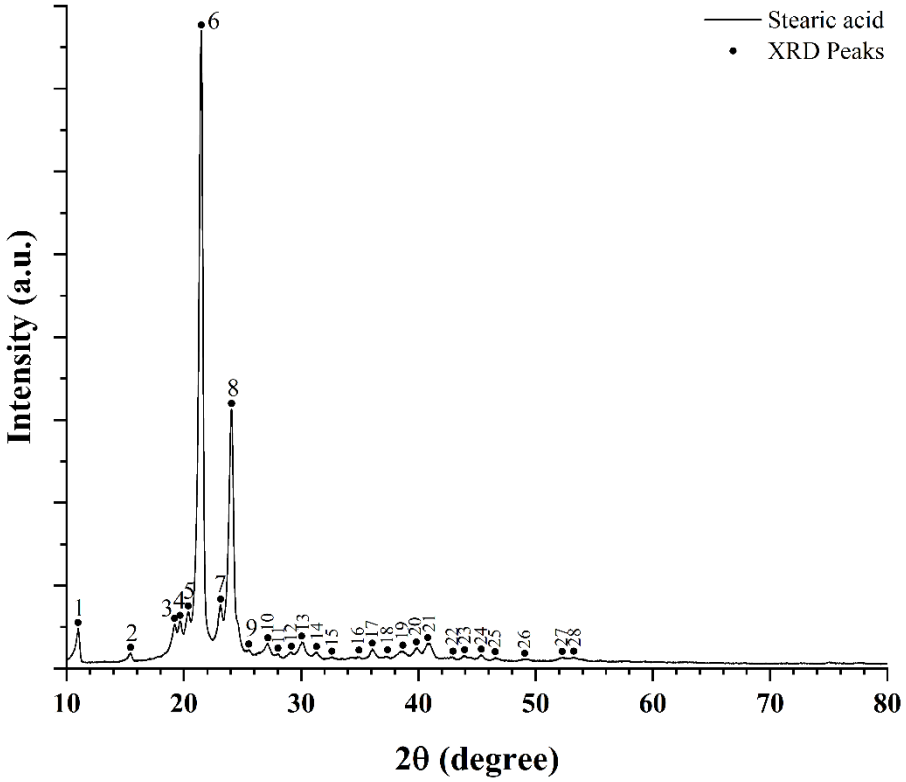

Figure 3. XRD pattern of stearic acid. XRD peaks are numbered with consecutive numbers from 1 to 28. XRD spectrum was recorded with step size of 0.02 degree.

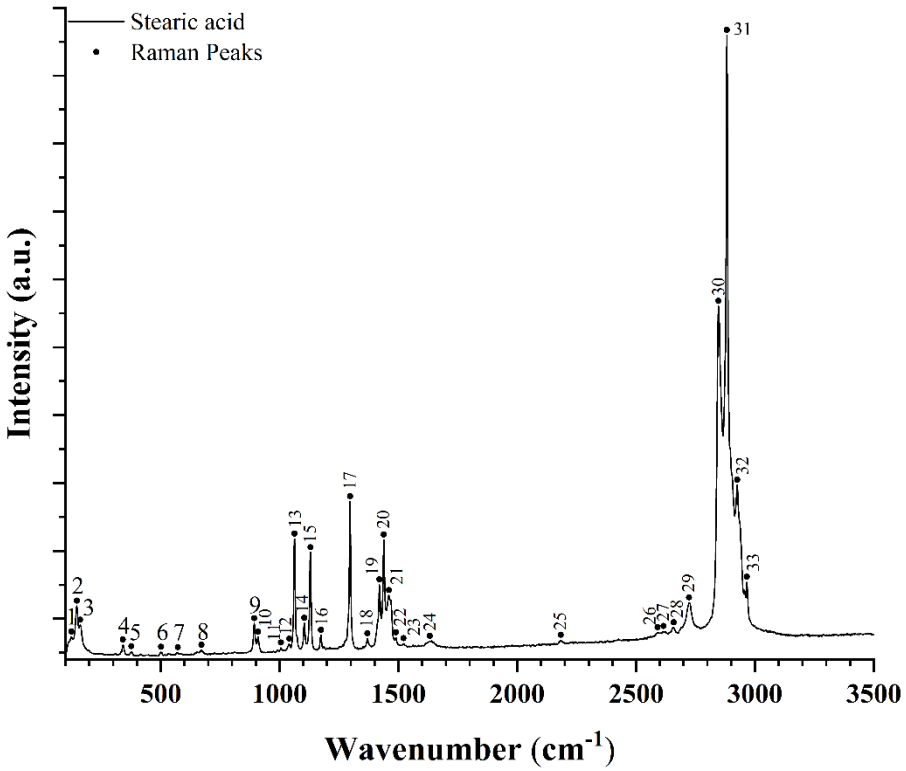

Figure 4. Raman spectrum of stearic acid. Stearic acid was excited with the wavelength of 633 nm. Raman peaks are numbered with consecutive numbers from 1 to 33.

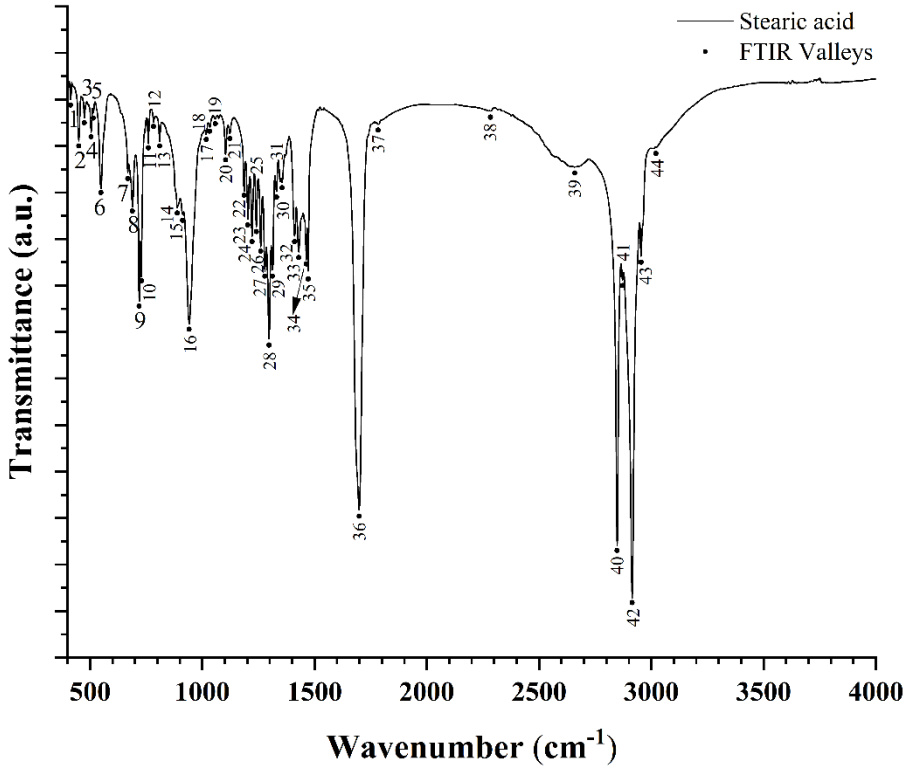

Figure 5. FTIR spectrum of stearic acid. FTIR bands are numbered with consecutive numbers from 1 to 44.

Table 2. Local maxima and minima derived from the Figure 2 to Figure 5. Bold written values indicate the strongest peaks and valleys in the spectrum.

Peaks and Valleys at The Spectra of Stearic Acid				
1st Derivative of TGA Temperature (ºC)	**XRD 2θ (º)**	**Raman Wavenumber (cm^{-1})**	**FTIR Wavenumber (cm^{-1})**	**Peak/Valley Row Number**
324.4	10.98	124.81	414	1
—	15.46	147.18	450	2
	19.22	161.616	475	3
	19.68	341.434	505	4
	20.38	377.081	515	5
	21.48	501.611	549	6
	23.14	572.258	668	7
	24.06	671.355	689	8
	25.54	893.311	**719**	9
	27.16	909.709	**729**	10
	28.02	1006.06	760	11
	29.18	1040.52	783	12
	30.04	**1063.39**	810	13
	31.32	1104.35	889	14
	32.62	**1130.37**	912	15
	34.94	1174.25	**942**	16
	36.08	**1296.35**	1018	17
	37.38	1369.53	1034	18
	38.68	1420.34	1058	19
	39.84	**1438.61**	1104	20

40.8	1460.04	1123	21
42.96	1489.91	1187	22
43.94	1521.74	1203	23
45.36	1631.82	1222	24
46.56	2182.78	1241	25
49.06	2590.58	1260	26
52.26	2615.79	1279	27
53.26	2658.13	**1298**	28
—	2723.09	1313	29
	2846.41	1331	30
	2881.91	1356	31
	2925.31	1411	32
	2965.91	1430	33
	—	1463	34
		1472	35
		1699	36
		1783	37
		2284	38
		2659	39
		2848	40
		2872	41
		2915	42
		2954	43
		3021	44

Stearic acid was used at the synthesis of different kinds of nanoparticles shown in Figure 6. These nanoparticles are composed of CdSe, Bi and Cu/Zn nanocrystals. TEM photos of CdSe nanoparticles are given at Figure 6a and 6b. In Figure 6b, white arrow shows one of these CdSe nanoparticles. Its size is approximately 4.4 nm and comparable to the exciton Bohr radius of CdSe (5.6 nm) [32]. For this reason, this semiconductor nanoparticle can be called as CdSe quantum dot. This condition is satisfied for all CdSe nanoparticles seen in Figure 6a and 6b. Average size of CdSe nanoparticles along with its standard deviation is found to be ~4.2±0.6 nm from Figure 6a. Therefore, these are CdSe quantum dots. Energy-dispersive X-ray (EDX) result of CdSe quantum dots is given at Figure 7a. Cd and Se elements were detected in these quantum dots. Core-shell quantum dots including CdSe have been used developing light emission diodes and fluorescent labels [33, 34]. Therefore, to synthesize these nanoparticles and investigate synthesis methods with different capping molecules have a technological importance. CdSe quantum dots are nearly spherical shape. TEM photo of a spherical Bi nanoparticle is seen at Figure 6c. It is indicated with dark blue arrow. Such a Bi nanoparticle is magnified at Figure 6d. It is almost spherical, and its size is ~123 nm. Mixed Cu/Zn nanoparticles are shown at Figure 6e. The size of the nanoparticle indicated by white arrow is ~12.2 nm. It is also a nanocrystal due to observation of its crystalline fringes. As seen from Figure 6, synthesis of CdSe quantum dots, Bi nanoparticles and mixed Cu/Zn nanocrystals have been achieved successfully by using stearic acid. Elemental composition of nanoparticles was confirmed with EDX (see Figure 7, Figure 8 and Figure 9). Elemental copper seen in Figure 7a and Figure 7b is caused by used TEM grid which is made of carbon film coated copper. Atomic percentages derived from EDX analysis of these nanoparticles are listed in Table 3. Figure 10 shows XRD spectrum of Cu/Zn nanocrystals. XRD peaks of this sample match well with those of stearic acid, pure copper, and pure zinc [35, 36]. There are no peaks related to oxide or alloy phases of copper and zinc in the spectrum [37, 38]. Therefore, it can be stated that these nanocrystals are a mixture of copper and zinc nanocrystals and capped with stearic acid.

Here, the role of stearic acid is explained as follows. Thermal decomposition of metal salt allows stearic acid molecules to attach metallic precursors during the synthesis. Then, metal stearate as an intermediate species comes out in the solution. Metal stearate can be decomposed alone and appearing metal ions in solution can be reduced, oxidized, or combined with other ions if it is desired. Zero-valent metals and

semiconductors at the nanometer scale can be synthesized by this way. Synthesis of metal nanoparticles or II-VI group semiconductor quantum dots (QDs) can be explained simply as follows [39-41].

$$Metal\ or\ Metal\ Salt + Stearic\ acid \rightarrow Metal - Stearate\ Complex \quad (1)$$

$$Metal - Stearate\ Complex \xrightarrow{Thermal\ decomposition} Metal\ Nanoparticles \quad (2)$$

$$Metal - Stearate\ Complex \xrightarrow{Injected\ TOPX\ (X=S,Se\ or\ Te)\ complex} II - VI\ Semiconductor\ QDs \quad (3)$$

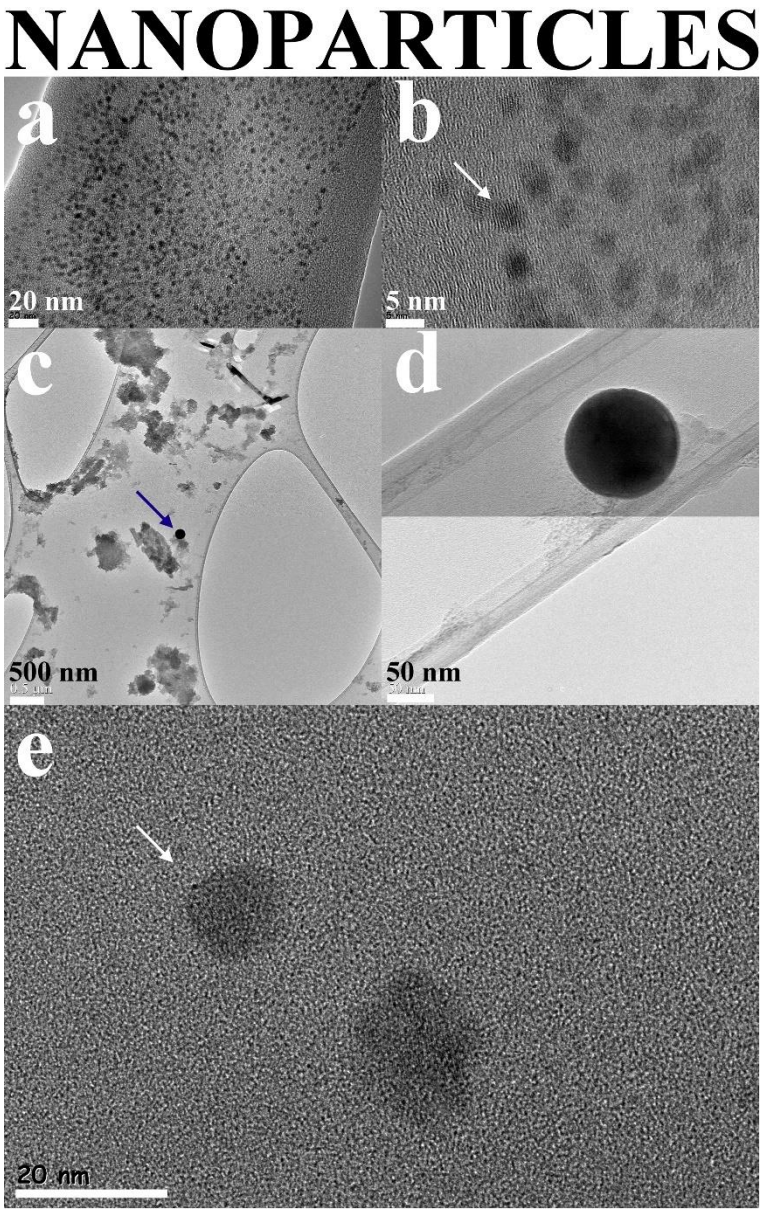

Figure 6. TEM photos of synthesized nanoparticles. (a): CdSe quantum dots, (b): CdSe quantum dots, white arrow shows a CdSe quantum dot, (c): Bi nanoparticle pointed out by dark blue arrow, (d): magnified image of a Bi nanoparticle similar to indicated at (c), and (e): mixed Cu/Zn nanocrystals, white arrow shows a Cu/Zn nanocrystal. Scale bar of these images is 20 nm (a), 5 nm (b), 500 nm (c), 50 nm (d), and 20 nm (e), respectively.

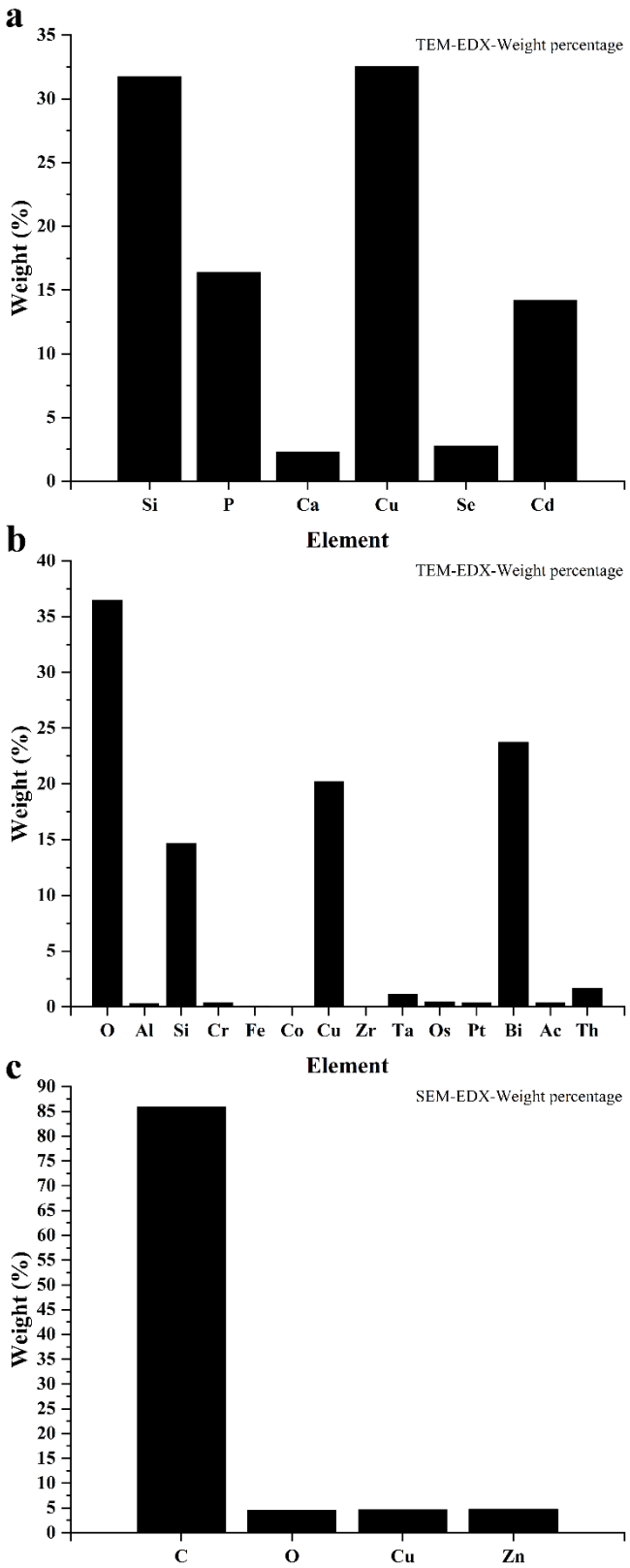

Figure 7. EDX weight percentage of elements. (a): CdSe quantum dots, (b): Bi nanoparticles and (c): Cu/Zn nanocrystals.

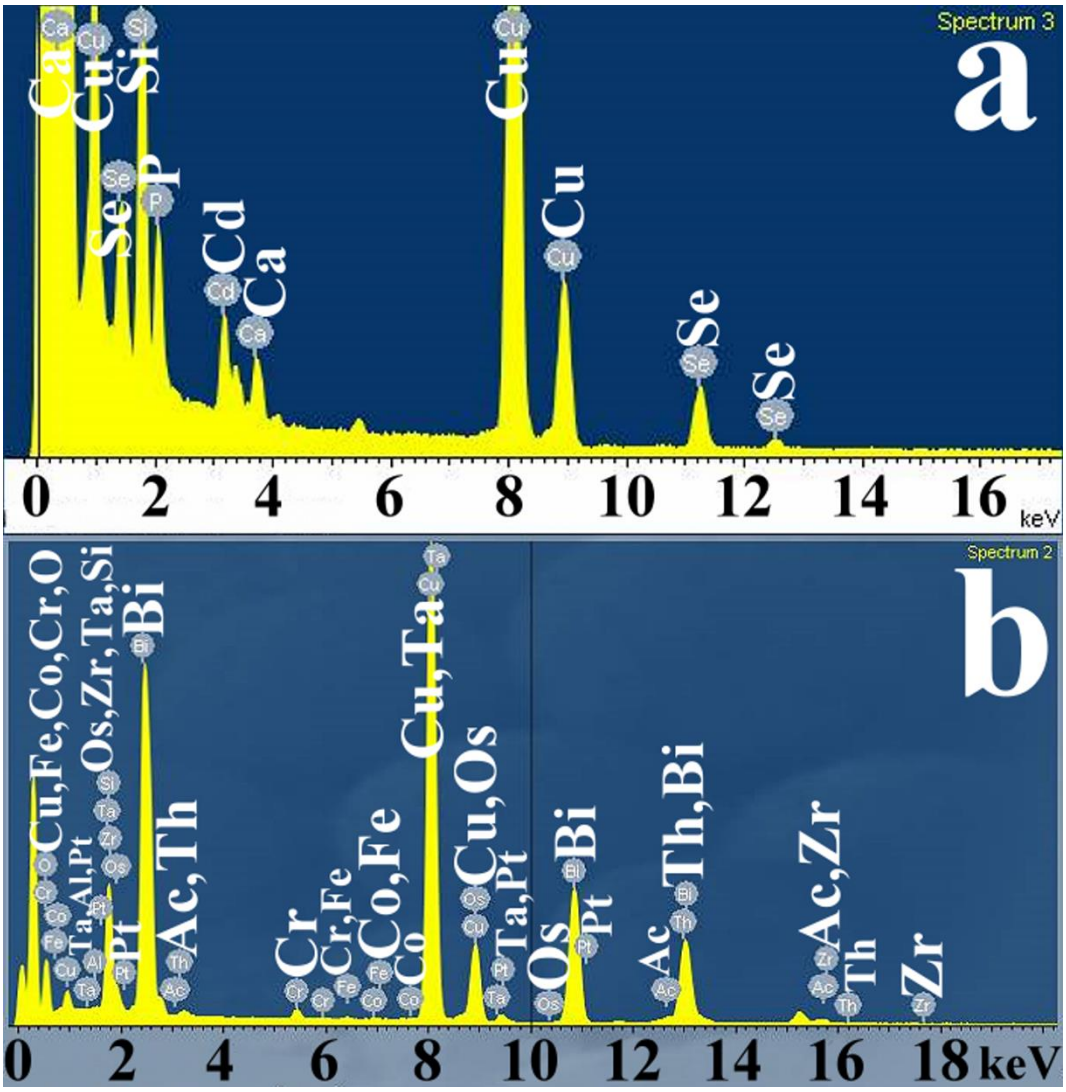

Figure 8. EDX spectra of CdSe quantum dots (a), and Bi nanoparticles (b).

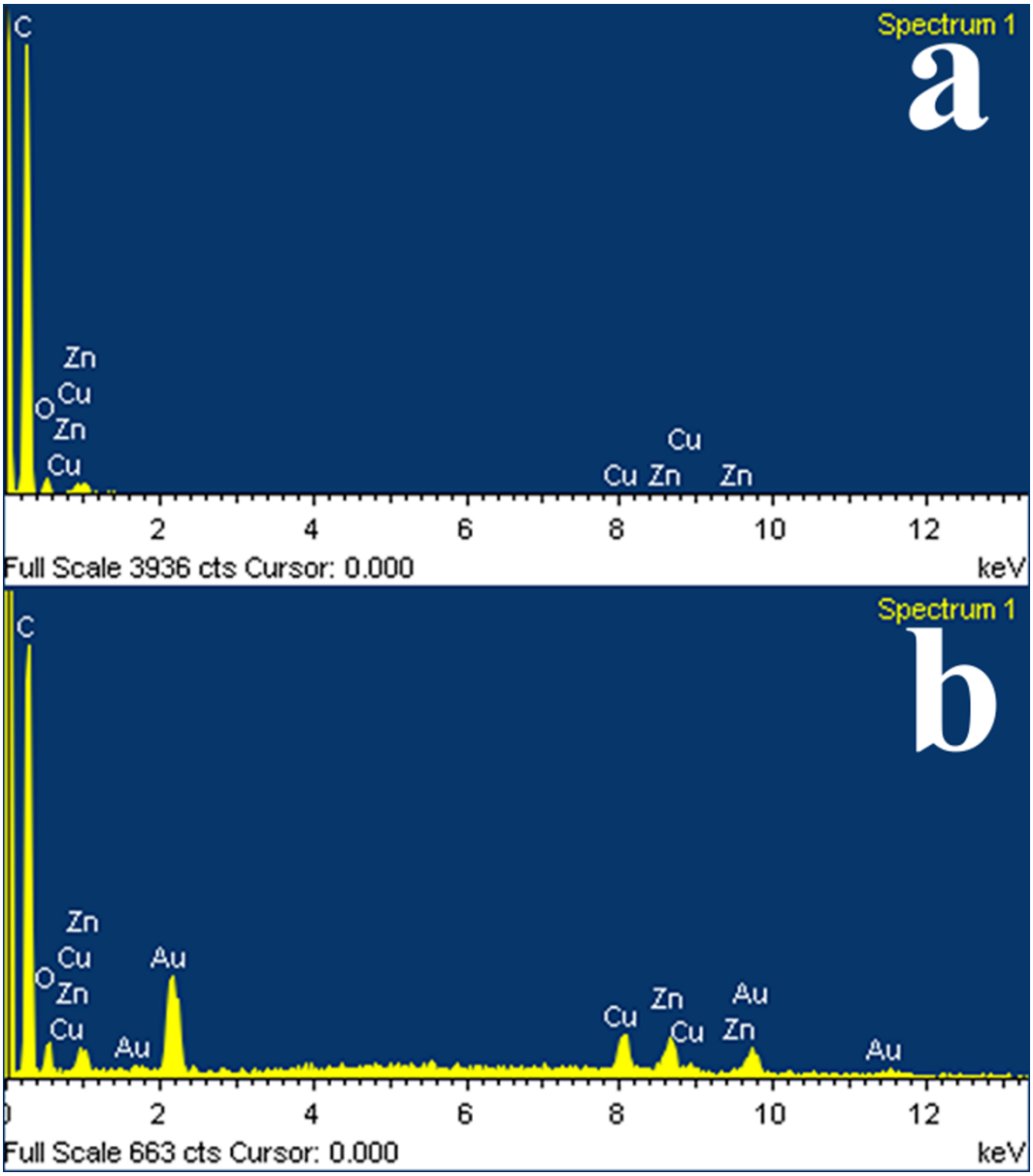

Figure 9. EDX spectra of Cu/Zn nanocrystals. (a): EDX analysis was performed without sample coating, and (b): EDX analysis was performed by coating the sample with a thin gold layer.

Table 3. EDX atomic percentages of CdSe quantum dots (QDs), Bi nanoparticles (NPs) and Cu/Zn nanocrystals (NCs).

	Atomic Percentage (%)		
Element	**CdSe QDs**	**Bi NPs**	**Cu/Zn NCs**
C	-	-	94.28
O	-	69.59	3.78
Al	-	0.37	-
Si	47.28	15.95	-
P	22.12	-	-
Ca	2.42	-	-
Cr	-	0.23	-
Fe	-	0.04	-
Co	-	0.03	-

Cu	21.42	9.70	0.97
Zn	-	-	0.97
Se	1.47	-	-
Zr	-	0.02	-
Cd	5.29	-	-
Ta	-	0.19	-
Os	-	0.08	-
Pt	-	0.06	-
Bi	-	3.47	-
Ac	-	0.05	-
Th	-	0.22	-

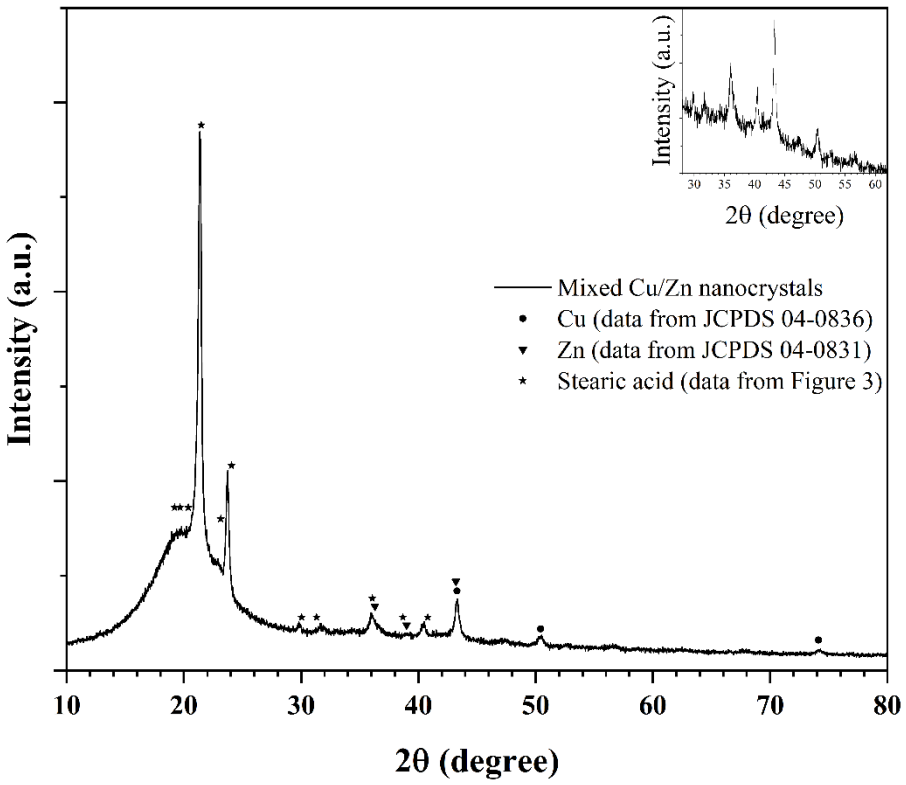

Figure 10. XRD spectrum of mixed Cu/Zn nanocrystals. XRD spectrum was recorded with step size of 0.02 degree. Inset figure shows its zoomed XRD spectrum between 28° and 62°.

4. CONCLUSION

Thermal decomposition of stearic acid was begun at ~286°C. Its two strongest XRD peaks were appeared at 21.48° and 24.06°. Symmetric and asymmetric vibrations of methylene groups of stearic acid were observed at 2846.41 cm^{-1} and 2881.91 cm^{-1} in its Raman spectrum, respectively, and 2848 cm^{-1} and 2915 cm^{-1} at its FTIR spectrum, respectively. Semiconductor CdSe quantum dots, semimetal Bi nanoparticles and mixed metal Cu/Zn nanocrystals were synthesized by using stearic acid. This study shows that many nanoparticles synthesized are nearly spherical and have a good crystallinity. Stearic acid was used as a good dispersant and capping agent to produce these nanoparticles.

ACKNOWLEDGEMENTS

This work was realized at Nanomaterial Production Laboratory of Toros University established within the scientific research project coded 2015-01-01-01-BAP-MUHF. TGA was performed at Central Research Laboratory of Çukurova University. FT-IR and Raman measurements were carried out at Central Laboratory of Middle East Technical University. TEM photos were taken at Research and Application Centre for Research Laboratories of Muğla Sıtkı Koçman University and Transmission Electron Microscopy Laboratory of Central Laboratory of Middle East Technical University. SEM-EDX measurements were made at Research and Application Centre for Research Laboratories of Muğla Sıtkı Koçman University.

CONFLICT of INTEREST

The author declares that there is no conflict of interest regarding the publication of this article.

REFERENCES

[1] Loften JR, Linn JG, Drackley JK, Jenkins TC, Soderholm CG, Kertz AF. Palmitic and stearic acid metabolism in lactating dairy cows. J Dairy Sci 2014; 97: 4661–4674. http://dx.doi.org/10.3168/jds.2014-7919

[2] Wang Q, Zhang B, Qu M, Zhang J, He D. Fabrication of superhydrophobic surfaces on engineering material surfaces with stearic acid. Appl Surf Sci 2008; 254: 2009–2012. https://doi.org/10.1016/j.apsusc.2007.08.039

[3] Wang H, Liang M, Gao J, He Z, Tian S, Li K, Zhao Y, Miao Z. Super-hydrophobic coating prepared by mechanical milling method. J. Coat. Technol. Res. 2021. https://doi.org/10.1007/s11998-021-00546-1

[4] Wu X, Yang F, Gan J, Kong Z, Wu Y. A superhydrophobic, antibacterial, and durable surface of poplar wood. Nanomaterials 2021; 11: 1-12. https://doi.org/10.3390/nano11081885

[5] Xu CL, Wang YZ. Self-assembly of stearic acid into nano flowers induces the tunable surface wettability of polyimide film. Materials and Design 2018; 138: 30-38. https://doi.org/10.1016/j.matdes.2017.10.057

[6] Gretić ZH, Mioč EK, Čadež V, Šegota S, Ćurković HO, Hosseinpour S. The influence of thickness of stearic acid self-assembled film on its protective properties. Journal of The Electrochemical Society 2016; 163: C937-C944. https://doi.org/10.1149/2.1461614jes

[7] Sarkar J, Pal P, Talapatra GB. Self-assembly of silver nano-particles on stearic acid Langmuir-Blodgett film: evidence of fractal growth. Chem Phys Lett 2005; 401: 400–404. https://doi.org/10.1016/j.cplett.2004.11.085

[8] Nguyen TT, Nguyen VK, Pham TTH, Pham TT, Nguyen TD. Effects of surface modification with stearic acid on the dispersion of some inorganic fillers in PE matrix. J Compos Sci 2021; 5: 1-9. https://doi.org/10.3390/jcs5100270

[9] Gilbert M, Petiraksakul P, Mathieson I. Characterisation of stearate/stearic acid coated fillers. Materials Science and Technology 2001; 17: 1472-1478. https://doi.org/10.1179/026708301101509494

[10] Hassabo AG, Sharaawy S, Mohamed AL. Saturated fatty acids derivatives as assistants materials for textile processes. Journal of Textile Science & Fashion Technology 2018; 1: 1-8. https://doi.org/10.33552/JTSFT.2018.01.000516

[11] Mostoni S, Milana P, Credico BD, D'Arienzo M, Scotti R. Zinc-based curing activators: new trends for reducing zinc content in rubber vulcanization process. Catalysts 2019; 9: 1-22. https://doi.org/10.3390/catal9080664

[12] Mensah MB, Awudza JAM, O'Brien P. Castor oil: a suitable green source of capping agent for nanoparticle syntheses and facile surface functionalization. R Soc open sci 2018; 5: 1-19. http://dx.doi.org/10.1098/rsos.180824

[13] Junkong P, Morimoto R, Miyaji K, Tohsan A, Sakaki Y, Ikeda Y. Effect of fatty acids on the accelerated sulfur vulcanization of rubber by active zinc/carboxylate complexes. RSC Adv 2020; 10: 4772-4785. https://doi.org/10.1039/C9RA10358A

[14] Taipale-Kovalainen K, Karttunen AP, Ketolainen J, Korhonen O. Lubricant based determination of design space for continuously manufactured high dose paracetamol tablets. European Journal of Pharmaceutical Sciences 2018; 115: 1-10. https://doi.org/10.1016/j.ejps.2017.12.021

[15] Dong C, Zhang X, Cai H, Cao C, Zhou K, Wang X, Xiao X. Synthesis of stearic acid-stabilized silver nanoparticles in aqueous solution. Advanced Powder Technology 2016; 27: 2416–2423. https://doi.org/10.1016/j.apt.2016.08.018

[16] Calvin JJ, Kaufman TM, Sedlak AB, Crook MF, Alivisatos AP. Observation of ordered organic capping ligands on semiconducting quantum dots via powder X-ray diffraction. Nature Communications 2021; 12: 1-8. https://doi.org/10.1038/s41467-021-22947-x

[17] Kaminski P, Przybylska D, Klima G, Grzyb T. Improvement in luminescence intensity of β-$NaYF_4$: 18%Yb^{3+}, 2%Er^{3+}@β-$NaYF_4$ nanoparticles as a result of synthesis in the presence of stearic acid. Nanomaterials 2022; 12: 1-16. https://doi.org/10.3390/nano12030319

[18] Altıntas Y, Talpur MY, Mutlugun E. The effect of ligand chain length on the optical properties of alloyed core-shell InPZnS/ZnS quantum dots. Journal of Alloys and Compounds 2017; 711: 335-341. https://doi.org/10.1016/j.jallcom.2017.03.326

[19] Rahmani M, Ghasemi FA, Payganeh G. Effect of surface modification of calcium carbonate nanoparticles on their dispersion in the polypropylene matrix using stearic acid. Mechanics & Industry 2014; 15: 63–67. https://doi.org/10.1051/meca/2014009

[20] Patti A, Lecocq H, Serghei A, Acierno D, Cassagnau P. The universal usefulness of stearic acid as surface modifier: applications to the polymer formulations and composite processing. Journal of Industrial and Engineering Chemistry 2021; 96: 1–33. https://doi.org/10.1016/j.jiec.2021.01.024

[21] Shen H, Wang H, Tang Z, Niu JZ, Lou S, Du Z, Li LS. High quality synthesis of monodisperse zinc-blende CdSe and CdSe/ZnS nanocrystals with a phosphine-free method. CrystEngComm 2009; 11: 1733-1738. https://doi.org/10.1039/B909063K

[22] Elsafi M, El-Nahal MA, Sayyed MI, Saleh IH, Abbas MI. Novel 3-D printed radiation shielding materials embedded with bulk and nanoparticles of bismuth. Sci Rep 2022; 12: 1-10. https://doi.org/10.1038/s41598-022-16317-w

[23] Gentzen M, Doronkin DE, Sheppard TL, Grunwaldt JD, Sauer J, Behrens S. Bifunctional catalysts based on colloidal Cu/Zn nanoparticles for the direct conversion of synthesis gas to dimethyl ether and hydrocarbons. Applied Catalysis A: General 2018; 557: 99-107. https://doi.org/10.1016/j.apcata.2018.03.008

[24] Kwon SG, Hyeon T. Formation mechanisms of uniform nanocrystals via hot-injection and heat-up methods. Small 2011; 7: 2685–2702. https://doi.org/10.1002/smll.201002022

[25] Allahverdi C. Synthesis and optical characterization of colloidal CdSe quantum dots nucleated for a long time at high temperature. Academic Platform Journal of Engineering and Science 2019; 7: 229-236. https://doi.org/10.21541/apjes.389919

[26] Allahverdi C, Erat S. Observation of nucleation and growth mechanism of bismuth nano/microparticles prepared by hot-injection method. Journal of Nano Research 2018; 54: 112-126. https://doi.org/10.4028/www.scientific.net/JNanoR.54.112

[27] Balkan T, Küçükkeçeci H, Zarenezhad H, Kaya S, Metin Ö. One-pot synthesis of monodisperse copper-silver alloy nanoparticles and their composition-dependent electrocatalytic activity for oxygen reduction reaction. Journal of Alloys and Compounds 2020; 831: 1-9. https://doi.org/10.1016/j.jallcom.2020.154787

[28] Martini WS, Porto BLS, de Oliveira MAL, Sant'Ana AC. Comparative study of the lipid profiles of oils from kernels of peanut, babassu, coconut, castor and grape by GC-FID and Raman spectroscopy. J Braz Chem Soc 2018; 29: 390-397. http://dx.doi.org/10.21577/0103-5053.20170152

[29] Silva LFL, Paschoal Jr W, Pinheiro GS, Filho JGS, Freire PTC, de Sousa FF, Moreira SGC. Understanding the effect of solvent polarity on the polymorphism of octadecanoic acid through spectroscopic techniques and DFT calculations. CrystEngComm 2019; 21: 297–309. https://doi.org/10.1039/C8CE01402G

[30] Oleszko A, Olsztyńska-Janus S, Walski T, Grzeszczuk-Kuć K, Bujok J, Gałecka K, Czerski A, Witkiewicz W, Komorowska M. Application of FTIR-ATR spectroscopy to determine the extent of lipid peroxidation in plasma during haemodialysis. BioMed Research International 2015; 2015: 1-8. https://doi.org/10.1155/2015/245607

[31] Vongsvivut J, Heraud P, Zhang W, Kralovec JA, McNaughton D, Barrow CJ. Quantitative determination of fatty acid compositions in micro-encapsulated fish-oil supplements using Fourier transform infrared (FTIR) spectroscopy. Food Chemistry 2012; 135: 603–609. https://doi.org/10.1016/j.foodchem.2012.05.012

[32] Guzelturk B, Martinez PLH, Zhang Q, Xiong Q, Sun H, Sun XW, Govorov AO, Demir HV. Excitonics of semiconductor quantum dots and wires for lighting and displays. Laser Photonics Rev 2014; 8: 73–93. https://doi.org/10.1002/lpor.201300024

[33] Chen W, Wang K, Hao J, Wu D, Qin J, Dong D, Deng J, Li Y, Chen Y, Cao W. High efficiency and color rendering quantum dots white light emitting diodes optimized by luminescent

microspheres incorporating. Nanophotonics 2016; 5: 565–572. https://doi.org/10.1515/nanoph-2016-0037

[34] Liu H, Tang W, Li C, Lv P, Wang Z, Liu Y, Zhang C, Bao Y, Chen H, Meng X, Song Y, Xia X, Pan F, Cui D, Shi Y. CdSe/ZnS quantum dots-labeled mesenchymal stem cells for targeted fluorescence imaging of pancreas tissues and therapy of type 1 diabetic rats. Nanoscale Research Letters 2015; 10: 1-12. https://doi.org/10.1186/s11671-015-0959-3

[35] Theivasanthi T, Alagar M. Nano sized copper particles by electrolytic synthesis and characterizations. International Journal of the Physical Sciences 2011; 6: 3662-3671.

[36] Velazquez-Gonzalez CE, Armendariz-Mireles EN, Pech-Rodriguez WJ, González-Quijano D, Rocha-Rangel E. Improvement of dye sensitized solar cell photovoltaic performance by using a ZnO-semiconductor processed by reaction bonded. Microsystem Technologies 2019; 25: 4567–4575. https://doi.org/10.1007/s00542-019-04476-2

[37] Manyasree D, Peddi KM, Ravikumar R. CuO Nanoparticles: Synthesis, characterization and their bactericidal efficacy. Int J App Pharm 2017; 9: 71-74. https://doi.org/10.22159/ijap.2017v9i6.71757

[38] Voncken JHL, Verkroost TW. Powder diffraction of cubic α-brass. Powder Diffr 1997; 12: 228-229. https://doi.org/10.1017/S0885715600009787

[39] Dou Q, Ng KM. Synthesis of various metal stearates and the corresponding monodisperse metal oxide nanoparticles. Powder Technology 2016; 301: 949–958. https://doi.org/10.1016/j.powtec.2016.07.037

[40] Banski M, Afzaal M, Malik MA, Podhorodecki A, Misiewicz J, O'Brien P. Special role for zinc stearate and octadecene in the synthesis of luminescent ZnSe nanocrystals. Chem Mater 2015; 27: 3797–3800. https://doi.org/10.1021/acs.chemmater.5b00347

[41] Bailey RE, Smith AM, Nie S. Quantum dots in biology and medicine. Physica E 2004; 25: 1–12. https://doi.org/10.1016/j.physe.2004.07.013